ISSN 1330-3651 (Print), ISSN 1848-6339 (Online)
https://doi.org/10.17559/TV-20230205000324
Preliminary communication

Wind Load of Low-Rise Building Based on Fluent Equilibrium Atmospheric Boundary Layer

Li ZHAO, Yuxue LI*

Abstract: The accurate simulation of the self-sustaining equilibrium atmospheric boundary layer is essential in computational wind engineering. In order to solve the problem of poor self-sustaining equilibrium atmospheric boundary layer, the method of adding source terms to the transport equation of the turbulence model was adopted to make the inlet profiles of average wind and turbulence wind consistent with the turbulence model. The consistency of the average wind profiles, turbulent characteristics of the three models at several different positions with and without considering the source terms were investigated respectively according to the corresponding CFD numerical example. Take the TTU low-rise building as an example, the proposed method of numerical simulations of the wind load on the structure surface. The results show that by adding source terms to the transport equations of the SST k-ω turbulence model can better achieve the self-sustaining of the atmospheric boundary layer. The velocity profiles and turbulence characteristics profiles of TTU low-rise building at the entrance and exit have high consistency when adding the source terms. The numerical simulation results of the wind pressure coefficient on the surface of the structure are in good agreement with the wind tunnel tests and field measurement results. It is shown that the method can effectively improve the accuracy simulation of the self-sustaining equilibrium of atmospheric boundary layer. The study conclusion proposes a new idea or research method for modeling the equilibrium atmosphere boundary layer and also provides further CFD simulations in structural wind engineering with theoretical and actual values.

Keywords: equilibrium atmosphere boundary layer; flow field characteristics; low-rise building; simulation; source term

1 INTRODUCTION

Computational fluid dynamics (CFD) is more and more widely used in civil engineering and other fields [1-4]. Accurate simulation of turbulence in the atmospheric boundary layer (ABL) is the premise and basis for CFD to study wind engineering problems. Therefore, reasonably simulating the equilibrium atmospheric boundary layer is one of the critical issues in the current numerical wind engineering research.

The building structures are generally located in the atmospheric boundary layer, if the equilibrium atmospheric boundary layer conditions are not satisfied in the numerical simulations [5], the inflow boundary conditions will change significantly before reaching the building, which increases the error of numerical calculation and reduces the reliability of numerical simulation. Many scholars at home and abroad have explored this. For example, Richard and Norris [6] proposed a set of inflow boundary conditions that approximately satisfy the equilibrium atmosphere boundary layer based on the standard k-ε model and discussed the values of relevant parameters in the turbulence model. Based on the standard k-ε model, Luo et al. [7] discussed inflow boundary conditions, turbulence model parameters, and additional source term models. Based on the standard k-ε model, Shi et al. [8] achieved the self-sustaining of the atmospheric boundary layer by adding source terms to the transport equations of turbulent kinetic energy and the dissipation rate and applying shear stress to the top and bottom boundary conditions of the flow field. Based on the standard k-ε model, Yang et al. [9] and Parente et al. [10] improved the accuracy of numerical simulation by changing the turbulence model parameters and adding wall roughness. Chao et al. [11] and Balogh and Parente [12] derived new mathematical models of the inflow boundary conditions with height, respectively, which better achieved the balance of the boundary layer flow field. Based on the Shear-Stress Transport (SST) turbulence model, Hu et al. adopted adding source terms to the turbulent kinetic energy and the specific dissipation rate transport equations to achieve accurate simulation in the equilibrium atmospheric boundary layer [13, 14]. To sum up, in recent years, the importance of balancing self-sustaining of the atmospheric boundary layer in wind engineering has gradually been accepted by people. The commonly used methods include correction of bottom and top boundary conditions, modification of turbulence model constants and addition of source terms. In this paper, the method of adding source terms to the transport equation of turbulent kinetic energy, dissipation rate or specific dissipation rate is used to make the inlet boundary conditions meet the turbulence equation, so as to achieve the self-sustainability of the simulated turbulent wind field and adapt to any inlet boundary conditions.

Based on the standard k-ε turbulence model, this paper adopts the inflow boundary conditions of the RH model [5] and Yangyi model [9], respectively, and the inflow boundary conditions based on the SST k-ω turbulence model. The method of adding source terms to the transport equations of the three models improves the self-sustaining effect of the atmospheric boundary layer. Through the secondary development of Fluent, the proposed method systematically studies the self-sustaining of the velocity and turbulence characteristics of the three models at different positions in the flow field without and with adding the source terms. On this basis, based on the analysis results, the turbulence model with a better effect in simulating the equilibrium atmospheric boundary layer is selected. Taking TTU low-rise building under 90 wind angle as an example, the numerical simulations of the surface wind load characteristics of the low-rise building without and with the addition of the source terms respectively, and extract the flow field under the above two cases. Explore the influence of adding source terms on the low-rise building structure, and the feasibility of the proposed method is verified comprehensively.

2 THE PROPOSAL OF THE METHOD

2.1 Governing Equation

In computational wind engineering (CWE), the governing equation of the flow around a bluff body is the viscous incompressible Navier-Stokes equation. The Reynolds Averaged Navier-Stokes (RANS) method is used to calculate the fluid governing equations [15].

$$\frac{\partial \rho}{\partial t}+\frac{\partial(\rho \bar{u}_i)}{\partial x_i}=0 \tag{1}$$

$$\frac{\partial\left(\rho \bar{u}_i\right)}{\partial t}+\frac{\partial(\rho \bar{u}_i \bar{u}_j)}{\partial x_j}=-\frac{\partial p}{\partial x_i}+\frac{\partial}{\partial x_j}\left(\mu \frac{\partial \bar{u}_i}{\partial x_j}-\rho \overline{u_i' u_j'}\right)+S_i \tag{2}$$

$$\frac{\partial\left(\rho \bar{\phi}\right)}{\partial t}+\frac{\partial(\rho \bar{u}_j \bar{\phi})}{\partial x_j}=\frac{\partial}{\partial x_j}\left(\Gamma \frac{\partial \bar{\phi}}{\partial x_j}-\rho \overline{u_j' \phi'}\right)+S \tag{3}$$

where, $\overline{u}$ is the turbulent mean velocity, P is the downwind pressure, ρ is the density of the fluid, $-\rho \overline{u_i' u_j'}$ is the Reynolds stress, μ is the power exposure, S_i is the generalized source term of the momentum equation, Γ is the effective diffusion coefficient of velocity, S is the generalized source term of the transport equation, ϕ is the generalized flow characteristic quantity of transport equation, $i, j = 1, 2, 3$.

Eq. (1) to Eq. (3) are the continuous equation, momentum equation, and scalar ϕ transport equation, respectively. New turbulence model equations close the RANS equations. There are two types of turbulence models: the Reynolds stress model (RSM) and the eddy-viscosity model. The eddy-viscosity model is divided into a zero-equation model, a one-equation model, and a two-equation model. The standard k-ε turbulence model and the SST k-ω model are representative two-equation models widely used in scientific research and engineering practice.

2.1.1 The Standard k-ε Turbulence Model

The standard k-ε turbulence model was proposed by Launder and Spalding [15]. It introduces k and ε based on the RANS equations to form the transport equations for k and ε. The governing equations of the standard k-ε turbulence model consist of the continuity equation (Eq. (1)), the momentum equation (Eq. (2)), and the transport equations for k and ε. The transport equations for k and ε are:

$$\frac{\partial(\rho k)}{\partial t}+\frac{\partial\left(\rho k u_i\right)}{\partial x_i}=\frac{\partial}{\partial x_j}\left[\left(\mu+\frac{\mu_t}{\sigma_k}\right)\frac{\partial k}{\partial x_j}\right] +G_k+G_b-\rho\varepsilon-Y_{\mathrm{m}}+S_k \tag{4}$$

$$\frac{\partial(\rho \varepsilon)}{\partial t}+\frac{\partial\left(\rho \varepsilon u_i\right)}{\partial x_i}=\frac{\partial}{\partial x_j}\left[\left(\mu+\frac{\mu_{\mathrm{t}}}{\sigma_\varepsilon}\right)\frac{\partial \varepsilon}{\partial x_j}\right] +C_{1\varepsilon}\frac{\varepsilon}{k}\left(G_k+C_{3\varepsilon}G_{\mathrm{b}}\right)-C_{2\varepsilon}\rho\frac{\varepsilon^2}{k}+S_\varepsilon \tag{5}$$

where, G_k is the production of turbulent kinetic energy, $G_k=u_t\left(\frac{\partial u_i}{\partial x_i}+\frac{\partial u_j}{\partial x_j}\right)\frac{\partial u_i}{\partial x_j}$, μ_t is the turbulent exposure, is defined as $u_t=\rho C_\mu \frac{k^2}{\varepsilon}$, μ is the power exposure, ρ_ε is the k of the dissipation term, Y_m is the fluctuating expansion term in the compressible turbulence, $Y_m = 0$, $C_{1\varepsilon}$, $C_{2\varepsilon}$, C_μ are the empirical constant, $C_{1\varepsilon} = 1.44$, $C_{2\varepsilon} = 1.92$, $C_\mu = 0.09$, σ_k, σ_ε are the Prandtl numbers corresponding to k and ε, respectively, $\sigma_k = 1.0$, $\sigma_k = 1.3$, S_k, S_ε are the user-defined source terms, other parameters have the same meaning as before.

2.1.2 The SST k-ω Turbulence Model

Menter [16] proposed the SST k-ω model, which takes advantage of the standard k-ω model [17] in the near-wall region and the standard k-ε in the far-field. The governing equations of the SST k-ω turbulence model can consist of the continuity equation (Eq. (1)), the momentum equation, and the transport equations for k and ω. The momentum equation and the transport equations for k and ω are:

$$\frac{\partial\left(\rho u_i\right)}{\partial t}+\frac{\partial(\rho u_i u_j)}{\partial x_j}=-\frac{\partial p}{\partial x_i}+\frac{\partial}{\partial x_j}\left(\Gamma\frac{\partial u_i}{\partial x_j}\right)+S_i \tag{6}$$

$$\frac{\partial(\rho k)}{\partial t}+\frac{\partial\left(\rho k u_i\right)}{\partial x_i}=\frac{\partial}{\partial x_j}\left[\Gamma_k\frac{\partial k}{\partial x_j}\right]+G_k-Y_k+S_k \tag{7}$$

$$\frac{\partial(\rho \omega)}{\partial t}+\frac{\partial\left(\rho \omega u_i\right)}{\partial x_i}=\frac{\partial}{\partial x_j}\left[\Gamma_\omega\frac{\partial \omega}{\partial x_j}\right]+G_\omega-Y_\omega+D_\omega+S_\omega \tag{8}$$

where, Γ, Γ_k, Γ_ω are the effective diffusion coefficient of velocity turbulent kinetic energy and specific dissipation rate, $\Gamma=\mu+\mu_t$, $\Gamma_k=\mu+\mu_t/\sigma_k$, $\Gamma_\omega=\mu+\mu_t/\sigma_\omega$, μ_t is the turbulent viscosity coefficient, $u_t=\frac{\rho_k}{\omega}\frac{1}{\max\left[1/\alpha^*, SF_2/\alpha_1\omega\right]}$, G_k, G_ω are the generic term of k and ω, $G_k=\min(\mu_t S^2, 10\rho\beta^* k\omega)$, $G_\omega=\alpha_\infty\rho S^2$, Y_k, Y_ω are dissipative terms of k and ω, $Y_k=\rho\beta^* k\omega$, $Y_m=\rho\beta_i\omega^2$, D_ω is the orthogonal dissipative term, $D_\omega=2\left(1-F_1\right)\rho\sigma_{\omega,2}\frac{1}{\omega}\frac{\partial k}{\partial x_j}\frac{\partial \omega}{\partial x_j}$, σ_k, σ_ω, α_∞, α^*, β^*, β_i are the coefficients in turbulence model, S is the tensor modulus of the average strain rate, F_1, F_2 are the mixed-function, S_i, S_k, S_ω are the user-defined source terms for each transport equations, other parameters have the same meaning as before.

2.2 Determination of Inflow Boundary Conditions and Source Terms of Transport Equations

As mentioned earlier, the setting of inflow boundary conditions has a more significant impact on the self-sustaining of the equilibrium atmospheric boundary layer. Under the existing inflow boundary conditions, k, ε, or ω

are difficult to satisfy their respective transport equations. Therefore, this paper proposed adding source terms to the turbulent transport equations to better self-sustaining the atmospheric boundary layer [18, 19]. The specific method is to substitute the expressions of velocity, turbulent kinetic energy, dissipation rate, or specific dissipation rate in the inflow boundary conditions into the transport equations of the turbulence model and derive the source term expressions of the turbulent kinetic energy, dissipation rate, or specific dissipation rate corresponding to each model.

2.2.1 Inflow Boundary Conditions and Source Terms Based on the Standard *k-ε* Turbulence Model

(1) RH model:

Richard and Hoxey [5] proposed a set of mathematical models with constant turbulent kinetic energy for boundary conditions (hereinafter referred to as the RH model). The specific expressions are as follows:

$$u = \frac{u_*}{\kappa}\ln\left(\frac{z+z_0}{z_0}\right) \tag{9}$$

$$k = \frac{u_*^2}{\sqrt{C_\mu}} \tag{10}$$

$$\varepsilon = \frac{u_*^3}{\kappa(z+z_0)} \tag{11}$$

Substitute Eq. (9) to Eq. (11) into Eq. (4) and Eq. (5), obtain the source term expressions of the model by mathematical derivation as [8]:

$$S_k = 0 \tag{12}$$

$$S_\varepsilon = \frac{\rho u_*^4\left[\sqrt{C_\mu}\sigma_\varepsilon(C_{2\varepsilon}-C_{1\varepsilon})-\kappa^2\right]}{\kappa^2\sigma_\varepsilon(z+z_0)^2} \tag{13}$$

where, u_* is the Friction velocity, κ is the von Karman constant, equal to 0.40 ~ 0.42, z_0 is the surface roughness length, C_μ is the standard *k-ε* turbulence model constant, C_μ = 0.09, other parameters have the same meaning as before.

(2) Yangyi model:

Yang et al. [9] derived a new set of inflow boundary conditions based on the simplified governing equations of the standard *k-ε* turbulence model. The specific expressions are as follows:

$$u = \frac{u_*}{\kappa}\ln\left(\frac{z+z_0}{z_0}\right) \tag{14}$$

$$k = \frac{u_*^2}{\sqrt{C_\mu}}\sqrt{C_1\ln\left(\frac{z+z_0}{z_0}\right)+C_2} \tag{15}$$

$$\varepsilon = \frac{u_*^3}{\kappa(z+z_0)}\sqrt{C_1\ln\left(\frac{z+z_0}{z_0}\right)+C_2} \tag{16}$$

Substitute Eq. (14) to Eq. (16) into Eq. (4) and Eq. (5), obtain the source term expressions of the model by mathematical derivation as [8]:

$$S_k = 0 \tag{17}$$

$$S_\varepsilon = \frac{\rho u_*^4}{\kappa^2\sigma_\varepsilon(z+z_0)^2}\times\left\{\kappa^2\left[\frac{3}{2}C_1-C_1\ln\left(\frac{z+z_0}{z_0}\right)-C_2\right]+\sqrt{C_\mu}\sigma_\varepsilon(C_{2\varepsilon}-C_{1\varepsilon})\sqrt{C_1\ln\left(\frac{z+z_0}{z_0}\right)+C_2}\right\} \tag{18}$$

where, C_1, C_2 are the fitting parameters, other parameters have the same meaning as before.

2.2.2 Inflow Boundary Conditions and Source Terms Based on the SST *k-ω* Turbulence Model

FLUENT provides several sets of turbulence boundary conditions for the SST *k-ω* turbulence model. This paper adopts a set of turbulence parameters of the often-used *k* and *ω*.

$$u = \frac{u_*}{\kappa}\ln\left(\frac{z+z_0}{z_0}\right) \tag{19}$$

$$k(z) = u_*^2\left[C_{u1}\ln\left(\frac{z+z_0}{z_0}\right)+C_{u2}\right]^2 \tag{20}$$

$$\omega(z) = \frac{u_*}{\kappa(z+z_0)}\left[C_{u1}\ln\left(\frac{z+z_0}{z_0}\right)+C_{u2}\right]^2 \tag{21}$$

Substitute Eq. (19) to Eq. (21) into Eq. (6) to Eq. (8), obtain the source term expressions of the model by mathematical derivation as [13]:

$$S_k = \frac{\rho u_*^3}{(z+z_0)}\times\left\{C_{1k}\left[C_{u1}\ln\left(\frac{z+z_0}{z_0}\right)+C_{u2}\right]^4-C_{2k}\right\} \tag{22}$$

$$S_\omega = \frac{\rho u_*^2}{(z+z_0)^2}\times\left\{C_{1\omega}\left[C_{u1}\ln\left(\frac{z+z_0}{z_0}\right)+C_{u2}\right]^4-C_{2\omega}\left[C_{u1}\ln\left(\frac{z+z_0}{z_0}\right)+C_{u2}\right]^2+C_{3\omega}\left[C_{u1}\ln\left(\frac{z+z_0}{z_0}\right)+C_{u2}\right]-C_{4\omega}\right\} \tag{23}$$

where, C_{u1}, C_{u2} are the turbulence boundary condition parameters, they can be obtained by fitting the experimental data, C_{1k}, C_{2k}, $C_{1\omega}$, $C_{2\omega}$, $C_{3\omega}$, $C_{4\omega}$ are the

introduced comprehensive coefficient, other parameters have the same meaning as before.

3 NUMERICAL MODEL FOR SELF-SUSTAINING OF ATMOSPHERIC BOUNDARY LAYER

3.1 Numerical Calculation Model

To verify the effectiveness of adding source terms to the transport equations of the turbulence model to realize the self-sustaining of the atmospheric boundary layer, numerical simulations of the three-dimensional airflow field. The length × width × height of the three-dimensional rectangular calculation domain is 12 m × 2 m × 2 m, use a structured grid to discretize the calculation domain (Fig. 1). The height of the first layer grid along the height direction near the ground is 0.01 m, the vertical grid growth factor is 1.05, the longitudinal and horizontal grids spacing is 0.1 m. The total number of grid cells is about 120000.

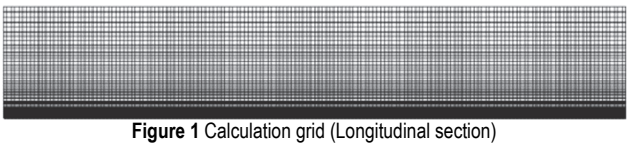

Figure 1 Calculation grid (Longitudinal section)

The inflow surface selects the velocity inlet boundary condition, the outflow surface selects the free outflow boundary condition, the top and both sides of the flow domain select the symmetrical boundary condition, and the surface and ground of the building select the wall condition without slip. The parameters in the boundary condition expression at the entrance are all obtained by fitting the wind tunnel test data [9, 20]. Obtained by data fitting:

$$u_* = 0.511 \text{ m/s}, \kappa = 0.42, z_0 = 0.000225,$$

$$C_1 = -1.36, C_2 = 12.3,$$

$$C_{u1} = -0.172, C_{u2} = 3.088,$$

$$C_{1k} = 0.10, C_{2k} = 0.64,$$

$$C_{1\omega} = 1.0, C_{2\omega} = C_{3\omega} = 0.0, C_{4\omega} = 0.02$$

Other model parameters adopt default values. A user-defined interface with Fluent realizes the entrance boundary. In Fluent, through User Defined Functions (UDF), DEFINE-PROFILE macros and F-PROFILE macros to achieve inflow boundary conditions, DEFINE-SOURCE macros to achieve additional source items.

The computational settings include the SIMPLEC algorithm for pressure-velocity coupling, and the discretization of the convection term adopts the second-order discretization format with high accuracy. The convergence criteria of the scaled residuals for all variables and continuity equation are set as 10^{-6}.

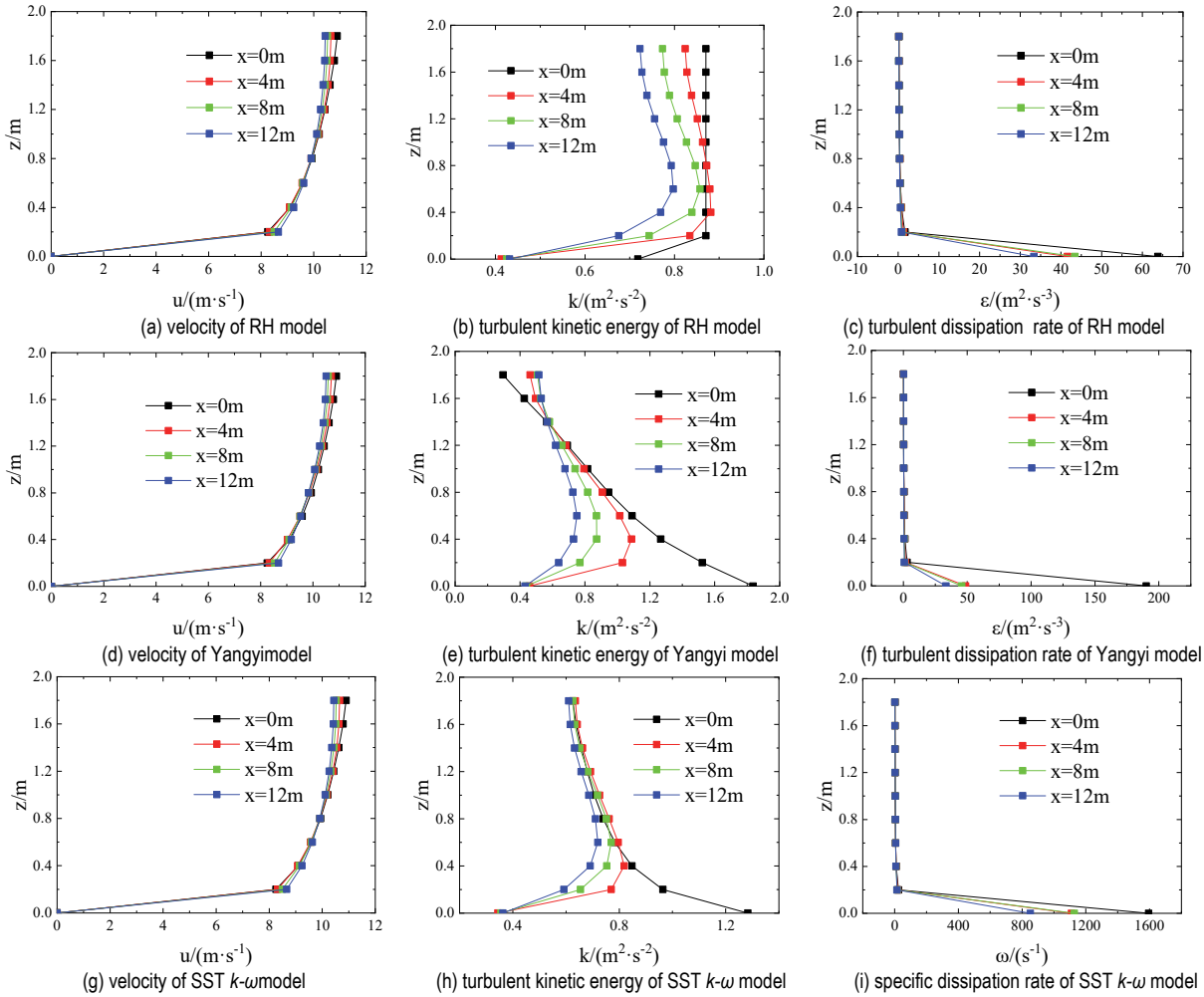

Figure 2 Velocity and turbulence characteristic profiles of different models and different positions without source term

3.2 Numerical Simulation Results

In order to compare the equilibrium atmospheric boundary layer self-sustaining effects of the RH model, the Yangyi model and the SST k-ω model listed in section 2.2, after the convergence of the flow field calculation, the key physical parameters of the velocity and turbulence characteristics profiles at four different locations along the longitudinal direction of the flow field, x = 0 m (at the entrance), x = 4 m (1/3 of the total length near the entrance), x = 8 m and x = 12 m (at the exit), were extracted and compared. Fig. 2 shows the curves of the velocity and turbulence characteristics profiles with height for the above three models at four different positions when not adding the source terms. Fig. 3 shows the curves of the velocity and turbulence characteristics profiles with height for the above three models at four different positions when adding source terms.

It can be seen from Fig. 2a, Fig. 2d, and Fig. 2g that when not adding the source terms, the velocity profiles of the three models are the same at four different locations, and the velocity profiles errors (based on the data at the entrance) are below 5%; however, the turbulence characteristics profiles errors (based on the data at the entrance) vary significantly. It can be seen from Fig. 2b and Fig. 2c that the maximum errors of the turbulent kinetic energy at other locations of the RH model relative to the entrance are below 15%, and the maximum errors of the dissipation rate at other locations relative to the entrance are below 20%. As we can see from Fig. 2e and Fig. 2f, when the height of the Yangyi model is 1.2 m ~ 1.4 m, the maximum errors of the turbulent kinetic energy at other locations relative to the entrance are below 5%. At other heights, k and ε at other locations are quite different from those at the entrance; in the area close to the ground, at the entrance, the turbulent kinetic energy is 1.8 m^2/s^2, and the dissipation rate is 190 m^2/s^3; at the exit, the turbulent kinetic energy is 0.5 m^2/s^2, and the dissipation rate is 40 m^2/s^3. They indicate that the flow field has not reached equilibrium at this time. As we can see from Fig. 2h and Fig. 2i, when the height of the SST k-ω model is greater than 0.4 m, k and ω at other locations are in good agreement with those at the entrance, and the errors (based on the data at the entrance) are below 8%. However, when the height is less than 0.4 m, k and ω at other locations are quite different from those at the entrance; in the area close to the ground, at the entrance, the turbulent kinetic energy is1.2 m^2/s^2, and the specific dissipation rate is 1500 s^{-1}; at the exit, the turbulent kinetic energy is 0.36 m^2/s^2, and the specific dissipation rate is 800 s^{-1}. They indicate that the flow field has not reached equilibrium at this time.

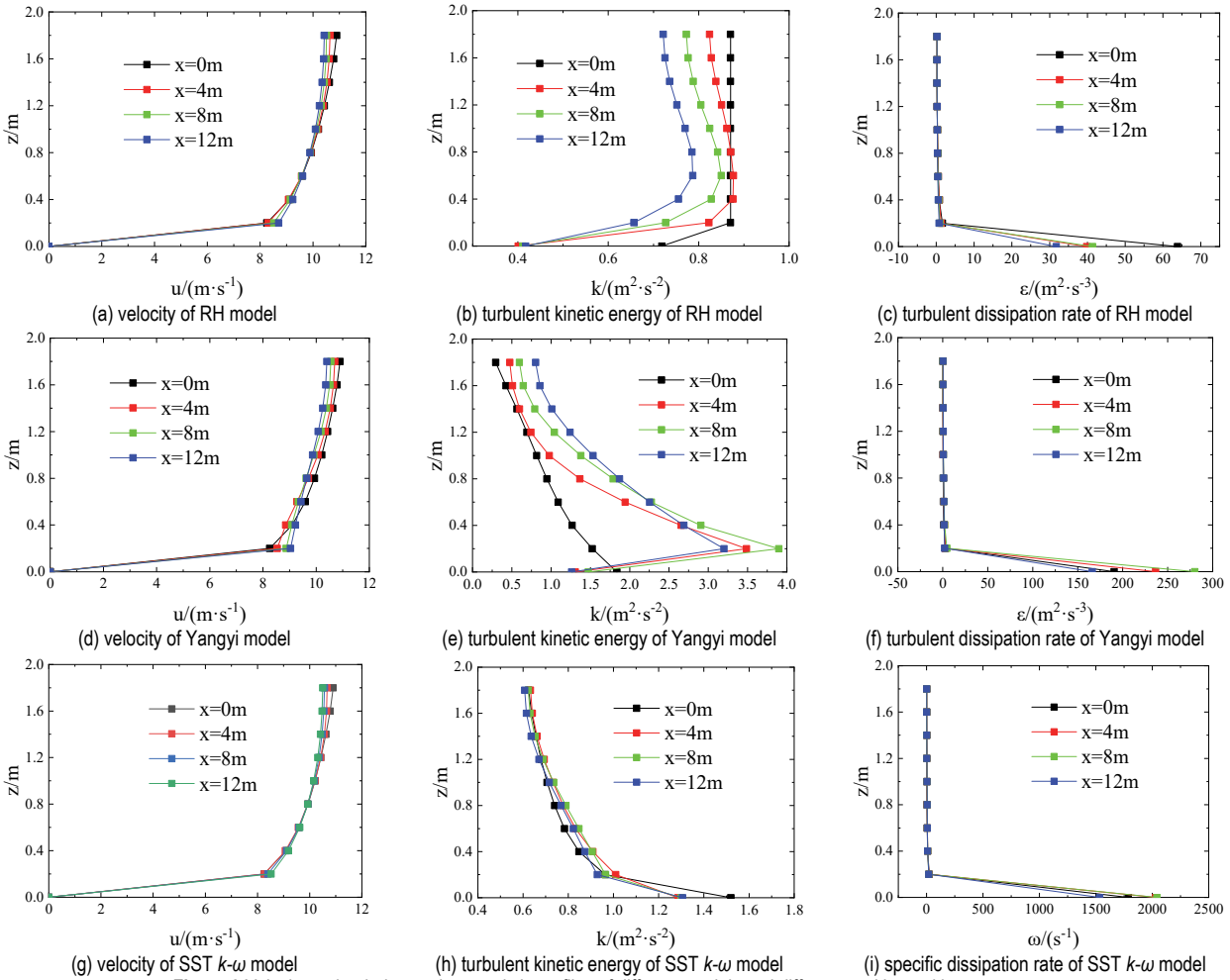

(a) velocity of RH model (b) turbulent kinetic energy of RH model (c) turbulent dissipation rate of RH model

(d) velocity of Yangyi model (e) turbulent kinetic energy of Yangyi model (f) turbulent dissipation rate of Yangyi model

(g) velocity of SST k-ω model (h) turbulent kinetic energy of SST k-ω model (i) specific dissipation rate of SST k-ω model

Figure 3 Velocity and turbulence characteristic profiles of different models and different positions with source term

It can be seen from Fig. 3a and Fig. 3d, and Fig. 3g that when adding the source terms, the velocity profiles of the three models maintain a high degree of consistency at four different locations, and the velocity profiles errors (based on the data at the entrance) are below 3%. It can be seen from Fig. 3b and Fig. 3c that the turbulence characteristics profiles of the RH model are not significantly improved compared to that without the source terms; the maximum errors of the turbulent kinetic energy at other locations relative to the entrance are below 13%, and the maximum errors of the dissipation rate at other locations relative to the entrance are below 17%. As we can see from Fig. 3e and Fig. 3f, the dissipation rate profiles of the Yangyi model are improved compared to that without source terms; the dissipation rate is 190 m^2/s^3 at the entrance and 160 m^2/s^3 at the exit, while the coincidence degree of the turbulent kinetic energy profiles near the ground is poor; for example, in the area close to the ground, the turbulent kinetic energy is 1.8 m^2/s^2 at the entrance and 1.2 m^2/s^2 at the exit. As we can see from Fig. 3h and Fig. 3i, after adding the source terms to the SST k-ω model, the turbulent kinetic energy can basically coincide everywhere, the errors (based on the data at the entrance) are below 5%, and the maximum errors of the specific dissipation rates at other locations relative to the entrance are below 10%, which meets the self-sustaining characteristics of the flow field.

Through the comparison of the flow field characteristic profiles without and with considering the source terms, it is shown that adding source terms to the transport equations of the SST k-ω turbulence model can obtain better equilibrium atmospheric boundary layer and achieve the self-sustaining characteristics of velocity, turbulent kinetic energy, and specific dissipation rate.

4 NUMERICAL SIMULATION OF LOW-RISE BUILDING MODEL

4.1 Low-Rise Building Model

In order to further verify the accuracy of the previous equilibrium atmospheric boundary layer in the numerical simulation of the actual flow field, the SST k-ω model, which is effective in simulating the equilibrium atmospheric boundary layer, is used to calculate the surface wind load characteristics of low-rise building. Select the standard model of the low-rise building in Texas Tech University (TTU) and numerically simulate the wind loads on the structure surface in two cases. Case 1 is the inflow boundary condition when not adding the source terms to the turbulence model transport equations (Eq. (19) to Eq. (21)), and case 2 is the inflow boundary condition when adding the source terms to the turbulence model transport equations (Eq. (19) to Eq. (23)). The length × width × height of the TTU model is 13.7 m × 9.2 m × 3.9 m, and there is a slope of 1/60 at the top, as shown in Fig. 4. Y represents the windward side, $T1$ and $T2$ represent the roof, and B represents the leeward side. The parameters in the boundary condition expressions at the entrance are obtained by fitting the wind tunnel test data [21].

The hybrid grid discretization method divides the computational domain into inner and outer parts: in the inner space near the model adopts tetrahedral elements, the grid is dense; in the outer space far away from the model adopts hexahedral elements, the grid is sparse.The total number of grids is about 500000. The solution settings are the same as those in section 3.1.

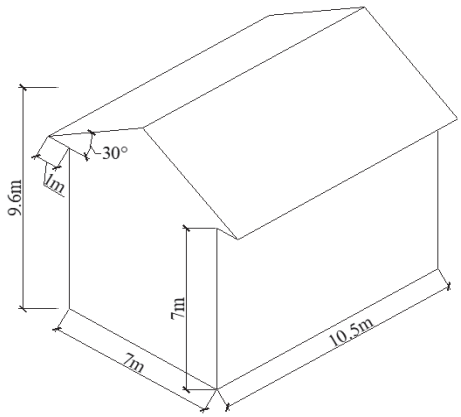

Figure 4 TTU model

The numerical simulation analyses the flow around the TTU model under 90 wind angles, then compares the two cases numerical simulation results with the field measured results [22] and the wind tunnel test results [21].

4.2 Analysis of Calculation Results

For the convenience of expression, extract the mean wind pressure P_i at i the measuring point, the static pressure P_0 at the reference point and the wind speed u_h at the reference point, substitute them into Eq. (24), it is treated as the dimensionless wind pressure coefficients corresponding to the wind pressure at the reference point by Eq. (24).

$$C_{p_i} = \frac{2\left(P_i - P_0\right)}{\rho u_h^2} \tag{24}$$

where, ρ is the fluid density, take 1.225 kg/m^3. The reference height is defined as the height of the eave position.

For the wind-resistant design of low-rise buildings, the shape coefficients of different structure surfaces are usually given [23]. Therefore, substitute Eq. (24) into Eq. (25) and convert it into shape coefficient through Eq. (25).

$$\mu_s = \sum_i \left[\left(\frac{10}{z_i} \right)^2 \frac{C_{P_i} A_i}{A} \right] \tag{25}$$

where, z_i is the i height of the measuring point, when $z_i < 10$, take 10.

Fig. 5 shows the comparison of the velocity, turbulent kinetic energy, and specific dissipation rate of the SST k-ω model at the entrance and exit in two cases, respectively. As we can see from Fig. 5, in case 2, the velocity profiles and turbulence characteristics profiles of the entrance and exit are in good agreement, indicating that the equilibrium atmospheric boundary layer simulation is well achieved at this time. In case 1, the velocity profiles of the entrance and exit are in good agreement, but the errors of the turbulence characteristics profiles are large, indicating that the flow field has not reached equilibrium at this time.

Fig. 6a shows the simulation results of the wind pressure coefficients on the surface of the building after treatment according to the Eq. (24). Fig. 6b shows the body shape coefficients of the different surfaces of the building structure after treatment according to Eq. (25) (where the locations of the different surfaces are shown in Fig. 4).

It can be seen from Fig. 6 that the simulation results of the wind pressure coefficients of case 2 are relatively close to the results of the wind tunnel test and field measurement, while there is a particular gap in the simulation results of case 1. For example, on the windward side *Y*, the variation range of the wind pressure coefficients of case 2 is 0.46 ~ 0.64, the body shape coefficient is 0.54, and the maximum errors of the wind pressure coefficients of case 2 (based on the wind tunnel test data) are about 10%. The variation range of the wind pressure coefficients of case 1 is 0.35 ~ 0.66, the body shape coefficient is 0.49, and the maximum errors of the wind pressure coefficients of case 1 (based on the wind tunnel test data) are about 15%. On roofs *T*1 and *T*2, the variation range of the wind pressure coefficients of case 2 is −1.6 ~ −0.24, the body shape coefficients are −0.72 ~ −0.39, and the maximum errors of the wind pressure coefficients of case 2 (based on the wind tunnel test data) are about 16%. The variation range of the wind pressure coefficients of case 1 is −1.6 ~ −0.34, the body shape coefficients are −1.05 ~ −0.49, and the maximum errors of the wind pressure coefficients of case 1 (based on the wind tunnel test data) are up to about 30%. In general, the simulation results of the wind pressure coefficients of case 2 agree well with the results of the wind tunnel test and field measurement. They are indicating that adding the source terms to the transport equations of the turbulence model can effectively improve the accuracy of the numerical simulation, which provides a basis for applying this method to the numerical calculation of wind loads on the low-rise building structure.

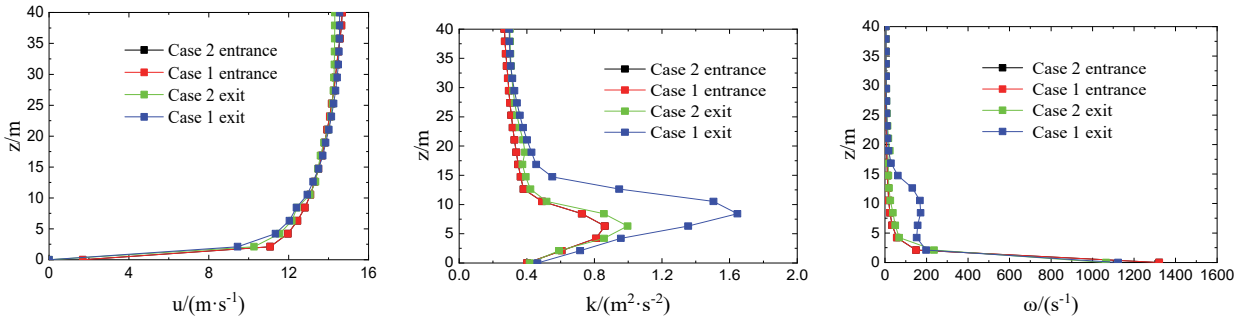

(a) velocity comparison (b) turbulent kinetic energy comparison (c) specific dissipation rate comparison

Figure 5 Velocity and turbulence characteristic profiles at the inlet and outlet of SST *k-ω* model

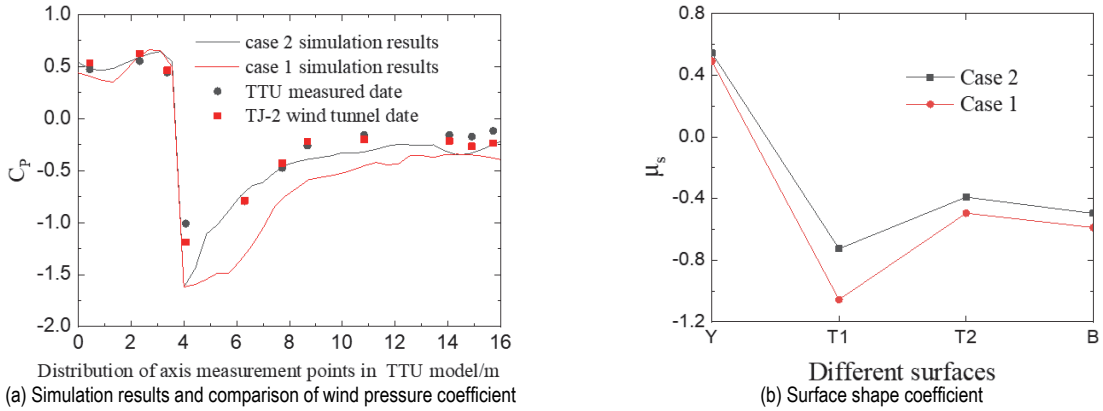

(a) Simulation results and comparison of wind pressure coefficient (b) Surface shape coefficient

Figure 6 Calculation results of wind load on the surface of low-rise building

4.3 Analysis of Flow Field Characteristics

To further explore the reasons for the influence of adding source terms on the surface wind field characteristics of the low-rise building, the wind flow field without and with the addition of source terms under 90 wind angle are compared and analyzed based on the numerical calculation results of the SST*k-ω* model for TTU low-rise building.

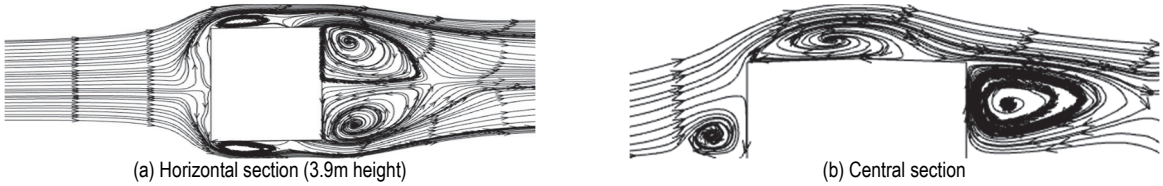

(a) Horizontal section (3.9m height) (b) Central section

Figure 7 Case 1 flow chart

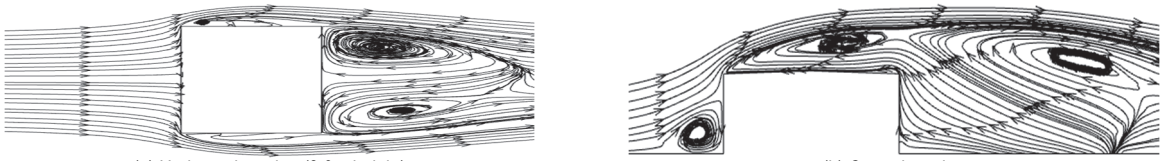

(a) Horizontal section (3.9m height) (b) Central section

Figure 8 Case 2 flow chart

Fig. 7 and Fig. 8 are streamlined diagrams of case 1 and case 2, respectively. As we can see from Fig. 7 and Fig. 8, in the two cases, the airflow separates on the windward side, about 2/3 of the height of the building. Part of the airflow flowing downward, forming an apparent vortex on the windward side of the building close to the ground, and part flowing upward along the windward side and over the top of the building (Fig. 7b, Fig. 8b); because the windward side obstructs the flow of airflow and is affected by pressure, the wind pressure value is positive (Fig. 6a). In case 1, the airflow produces a relatively small vortex near the front edge of both sides of the low-rise building (Fig. 7a), which causes a significant change in wind pressure on both windward sides compared to case 2 (Fig. 8a). In both cases, the airflow forms a vortex on the roof, case 1 vortex is near the ridge of the roof T1 (Fig. 7b), and case 2 vortex is near the roof T2 (Fig. 8b), and the vortex centre is closer to the building in case 1 than case 2. The vortex will have a strong suction effect on the roof, resulting in more significant negative wind pressure on the roof in case 1 than in case 2 (Fig. 6a). The airflow around the low-rise building forms two obvious reflux vortices on the leeward side; compared with case 1, case 2 has a larger vortex range, and the vortex centre is farther from the building (Fig. 7a, Fig. 8a). The separation of airflow forms a series of discrete vortices, and very large suction forces appear at the central of these vortices [24], which is the main reason for the extreme value of local wind pressure (suction) on the surface of the building. As the vortex centre of case 1 is close to the building, the absolute value of negative wind pressure on the roof of case 1 is more significant than that of case 2, consistent with the results of Fig. 6a. As we can see from Fig. 6a, the wind pressure distribution on the roof of case 2 is closer to the wind tunnel test value, resulting from the wind pressure change caused by the difference between the vortices of the two cases. In summary, when adding the source terms, the numerical calculations accurately reflect the wind pressure distribution on the surface of the TTU low-rise building structure, which further verifies the effectiveness of the proposed method.

5 CONCLUSIONS

(1)The turbulence characteristics profiles of the RH model are not significantly improved when adding the source terms compared with that without adding the source terms. The dissipation rate profiles of the Yangyi model are significantly improved when adding the source terms, but the turbulent kinetic energy profiles are poorly fitted near the ground. The turbulent kinetic energy and specific dissipation rate of the SST k-ω model are significantly improved after adding the source terms, which can better satisfy the flow field self-sustaining, which verifies the effectiveness of the proposed method to achieve the self-sustaining of the atmospheric boundary layer.

(2) The SST k-ω turbulence model has a better effect on simulating the equilibrium atmospheric boundary layer than other models. The SST k-ω turbulence model is selected to simulate and analyze the TTU low-rise building under 90 wind angle when adding source terms and not adding source terms. The results show that: the velocity profiles and turbulence characteristics profiles have high consistency when adding the source terms, which can better achieve the balance of the atmospheric boundary layer. The simulation results when adding the source terms are in good overall agreement with the wind tunnel test and field measurement results, indicating that the method effectively improves the accuracy of numerical simulation and provides a basis for the application of the method to the numerical calculation of structural wind loads.

(3) The flow fields around the two cases are compared and analyzed based on the numerical calculation results above. The similarities between the two cases, the airflow creates powerful vortices below the front stationing point, above the roof, and on the leeward side of the TTU low-rise building. The difference between the two cases, comparing the airflow vortex above the roof and at the leeward side, in Case 2, the vortex range is more extensive, and the vortex location is farther from the building. The closer the centre of the vortex is to the building, the greater the wind suction force is generated, resulting in a larger absolute value of negative wind pressure on the roof of case 1 than that of case 2, which is consistent with the results in Fig. 6a.

Acknowledgment

These authors gratefully acknowledge the support of the National Science Foundation of Hebei Province (Grant No.: E2019210031), the support of the Hebei Provincial Department of Science and Technology (Grant No.: 206Z5401G), the support of the Hebei Provincial Department of Education (Grant No.: QN2023195). the support of the Open Project of Beijing Key Laboratory of Structural Wind Engineering and Urban Wind Environment, Beijing Jiaotong University (Grant No.: 2023-1).

6 REFERENCES

[1] Ridha, H. & Al-Abboodi, N. K. F. (2022). Two-Phase Liquid-Solid Hydrodynamics of Inclined Fluidized Beds. *Power Engineering and Engineering Thermophysics*, *1*(1), 33-47. https://doi.org/10.56578/peet010105

[2] Lops, C., Germano, N., Ricciutelli, A., D'Alessandro, V., & Montelpare, S. (2021). Naturally ventilated double skin façades: Comparisons between different CFD models.

Mathematical Modelling of Engineering Problems, *8*(6), 837-846. https://doi.org/10.18280/mmep.080601
[3] Abdullah, K. A. & Barwari R. R. I. (2022). CFD simulation of thermal plume of vrf air conditioners for cooling season in semi-closed spaces for Erbil climate conditions. *International Journal of Heat and Technology*, *40*(4), 1079-1085. https://doi.org/10.18280/ijht.400426
[4] Song, L. Z., Zhu, J., Liu, S. T., & Qu, Z. J. (2022). Recent Fire Safety Design of High-Rise Buildings. *Journal of Urban Development and Management*, *1*(1), 38-46. https://doi.org/10.56578/judm010106
[5] Richard, P. J. & Hoxey, R. P. (1993). Appropriate boundary conditions for computational wind engineering models using the k-ε turbulence model. *Journal of Wind Engineering and Industrial Aerodynamics*, *46-47*, 145-153. https://doi.org/10.1016/0167-6105(93)90124-7
[6] Richard, P. J. & Norris, S. E. (2011). Appropriate boundary conditions for computational wind engineering models revisited. *Journal of Wind Engineering and Industrial Aerodynamic*, *99*(4), 257-266. https://doi.org/10.1016/j.jweia.2010.12.008
[7] Luo, K. W., Yang, Y., & Xie, Z. N. (2018). A comparative study on the simulation of neutral atmospheric boundary layer based on the k-ε turbulence model. *Engineering Mechanics*, *35*(2), 21-29.
[8] Shi, B. T., Zhang, X. B., & Huang, W. F. (2019). Equilibrium atmospheric boundary layer simulation based on standard model. *Journal of Hefei University of Technology (Natural Science*, *42*(8), 1106-1113. https://doi.org/10.1088/1475-7516/2019/08/017
[9] Yang, Y., Gu, M., Chen, S. Q., & Jin, X. Y. (2009). New inflow boundary conditions for modelling the neutral equilibrium atmospheric boundary layer in computational wind engineering. *Journal of Wind Engineering and Industrial Aerodynamics*, *97*(2), 88-95. https://doi.org/10.1016/j.jweia.2008.12.001
[10] Parente, A., Gorle, C., van Beeck, J., & Benocci, C. (2011). A comprehensive modelling approach for the neutral atmospheric boundary layer: Consistent inflow conditions wall function and turbulence model. *Boundary-Layer Meteorology*, *140*(3), 411-428. https://doi.org/10.1007/s10546-011-9621-5
[11] Chao, L., Xiao, Y., & Liu, A. (2015). Revisiting the CFD modelling horizontally homogenous atmospheric boundary layer. *14th International Conference on Wind Engineering Porto Alegre*, Porto Alegre, Brazil, April.
[12] Balogh, M. & Parente, A. (2015). Realistic boundary conditions for the simulation of atmospheric boundary layer flows using an improved k-ε model. *Journal of Wind Engineering and Industrial Aerodynamics*, *144*, 183-190. https://doi.org/10.1016/j.jweia.2015.01.010
[13] Hu, P., Li Y. L., & Liao, H. L. (2012). Simulation of equilibrium atmosphere boundary layer with SST k-ε turbulence model. *Acta Aerodynamica Sinica*, *30*(6), 737-743.
[14] Hu, P., Li, Y. I., Yan, H., Steve, C. S., & Xu, X. Y. (2016). Numerical simulations of the mean wind speeds and turbulence intensities over simplified gorges using the SST k-ε turbulence model. *Engineering Applications of Computational Fluid Mechanics*., *10*(1), 361-374. https://doi.org/10.1080/19942060.2016.1169947
[15] Launder, B. E. & Spalding, D. B. (1972). Lectures in Mathematical Models of Turbulence. *Academic Press*, London, UK.
[16] Wilcox, D. C. (1988). Multiscale model for turbulent flows. *AIAA Journal*, *26*(11), 1311-1320. https://doi.org/10.2514/3.10042
[17] Menter, F. R. (1994). Two-equation eddy-viscosity turbulence models for engineering applications. *AIAA Journal*, *32*(8), 1598-1605. https://doi.org/10.2514/3.12149
[18] Parente, A., Gorle, C., van Beeck, J., & Benocci, C. (2011). Improved k-ε model and wall function formulation for the RANS simulation of ABL flows. *Journal of Wind Engineering and Industrial Aerodynamics*, *99*(4), 267-278. https://doi.org/10.1016/j.jweia.2010.12.017
[19] Hu, P. (2013). *Study on wind characteristics at bridge site in a deep-cutting gorge by wind tunnel test and CFD method*. PhD. Dissertation, Southwest Jiaotong University, Sichuan, China.
[20] Yang, W. (2004). *Numerical simulation study of structural wind load and response based on RANS*. PhD. Dissertation, Tongji University, Shanghai, China.
[21] Gu, M., Yang, W., Huang, P., & Luo, P. (2006). Wind tunnel test andnumerical simulation on TTU building model. *Journal of Tongji University (Natural Science)*, *34*(12), 1563-1567.
[22] Levitan, M. L., Mehta, K. C., Vann, W. P., & Holmes, J. D. (1991). Field measurements of pressure on the texastech building. *Journal of Wind Engineering and Industrial Aerodynamics*, *38*(2-3), 227-234. https://doi.org/10.1016/0167-6105(91)90043-v
[23] Load Code for the Design of Building Structures. GB50009-2019. (2019). Ministry of Construction, China.
[24] Kawai, H. (1997). Structure of conical vortices related with suction fluctuation on a flat roof in oblique smooth and turbulent flows. *Journal of Wind Engineering and Industrial Aerodynamics*, *69-71*, 579-588. https://doi.org/10.1016/s0167-6105(97)00188-8

Contact information:

Li ZHAO
School of Civil Engineering,
Shijiazhuang Tiedao University,
Shijiazhuang 050043, China
Hebei Vocational College of Labour Relations.
Shijiazhuang 050093, China
E-mail: zl201987@163.com

Yuxue LI
(Corresponding author)
School of Civil Engineering,
Innovation Center for Wind Engineering and Wind Energy Technology of Hebei Province,
Key Laboratory of Roads and Railway Engineering Safety Control of China Ministry of Education,
Shijiazhuang Tiedao University,
Shijiazhuang 050043, China
E-mail: liyuxue2000@163.com